

Frank-Wolfe Stein Sampling

Futoshi Futami
The University of Tokyo, RIKEN
futami@ms.k.u-tokyo.ac.jp

Zhenghang Cui
The University of Tokyo, RIKEN
cui@k.u-tokyo.ac.jp

Issei Sato
The University of Tokyo, RIKEN
sato@k.u-tokyo.ac.jp

Masashi Sugiyama
RIKEN, The University of Tokyo
sugi@k.u-tokyo.ac.jp

Abstract

In Bayesian inference, the posterior distributions are difficult to obtain analytically for complex models such as neural networks. Variational inference usually uses a parametric distribution to approximate, from which we can easily draw samples. Recently discrete approximation by particles has attracted attention because of its expressive ability. An example is Stein variational gradient descent (SVGD), which iteratively optimizes particles. Although SVGD has been shown to be computationally efficient empirically, its theoretical properties have not been clarified yet and no finite sample bound of a convergence rate is known. Another example is Stein points (SP), which minimizes kernelized Stein discrepancy directly. The finite sample bound of SP is $\mathcal{O}(\sqrt{\log N/N})$ for N particles, which is computationally inefficient empirically, especially in high-dimensional problems. In this paper, we propose a novel method named *Frank-Wolfe Stein sampling*, which minimizes the maximum mean discrepancy in a greedy way. Our method is computationally efficient empirically and theoretically achieves a faster convergence rate, $\mathcal{O}(e^{-N})$. Numerical experiments show the superiority of our method.

1 Introduction

Approximating the expectation of a function $f(x)$ over a probability distribution $p(x)$ is a common problem in machine learning [4]:

$$Z_{f,p} = \int f(x)p(x)dx. \quad (1)$$

For example, in Bayesian inference, $f(x)$ is usually the likelihood, and $p(x)$ is a prior distribution or a posterior distribution. In many cases, analytical expression of the integral cannot be obtained, thus we need approximation methods.

In this paper, we focus on the case where $p(x)$ is a posterior distribution or an unnormalized distribution. Variational inference (VI) is widely used as an approximation method [5]. VI approximates the target distribution with a parametric distribution, from which we can easily draw samples. In VI, we often consider the mean field assumption and use parametric models based on exponential families [5]. Since these assumptions are used to make optimization more tractable, they are often too restrictive to approximate the target distribution. Therefore, the approximate distribution

Table 1: Comparison of discrete approximation methods for unnormalized distributions. Convergence rate is the order that an approximate distribution converges in distribution to the target distribution. Optimization method means how particles are updated. Computational cost per iteration is order of computation for calculating gradients or evaluating grid search samples.

Method	SVGD	Stein points	FWSS (Ours)
Convergence rate	Unknown	$\mathcal{O}(\sqrt{\log N/N})$	$\mathcal{O}(e^{-N})$
Optimization method	Batch learning Gradient descent	Incremental learning Sampling and Grid Search	Incremental learning Gradient descent
Computational cost per iteration	$\mathcal{O}(N^2)$	$\mathcal{O}(N)$	$\mathcal{O}(N)$
Number of evaluations of $\nabla_x \log p(x)$ per iteration	N	$4N$	N

never converges to the target distribution in general, which means that the approximation of Eq.(1) is biased, and no theoretical guarantee is assured.

An alternative way is a discrete approximation of the target distribution by using a set of particles [4], $\hat{p}(x) = \sum_{n=1}^N \delta(x - x_n)/N$, where N is the number of the particles and δ is the Dirac delta function. Particle approximation is free of VI assumptions and more expressive. The Monte Carlo (MC) method is used to draw particles randomly and independently [4]. However, the drawback of MC is that vast computational resources are required to sample from multi-modal and high-dimensional distributions.

Recently, methods that optimize particles through iterative updates have been proposed. One example is Stein variational gradient descent (SVGD) [26], which iteratively updates all particles in the direction that is characterized by kernelized Stein discrepancy (KSD). The update is actually implemented by gradient descent and can work well in high-dimensional problems. The computational cost of SVGD is $\mathcal{O}(N^2)$ per iteration. However, theoretical properties of SVGD have not been clarified and no finite sample bound of the convergence rate is known [23]. Another example is the Stein points (SP) method [8], which directly minimizes KSD. Although this method is assured by a finite sample bound, it is not practically feasible in high-dimensional problems due to the curse of dimensionality, because gradient descent is not available and sampling or grid search is used. Moreover, the number of evaluations of $\nabla_x \ln p(x)$, which usually requires vast computational cost, is four times of that of SVGD. The properties of existing methods are summarized in Table 1.

We aim to develop a discrete approximation method that is computationally efficient, works well in high-dimensional problems, and also has a theoretical guarantee for the convergence rate. To this end, we propose *Frank-Wolfe Stein sampling (FWSS)*, which is a greedy optimization method that directly minimizes maximum mean discrepancy (MMD) [13]. Our convex formulation of a discrete approximation enables us to use the Frank-Wolfe (FW) algorithm [17] and to derive a finite sample bound of the convergence rate. Remarkably, we show much faster convergence, linear convergence compared to SP (see Table 1 again).

Our contributions in this paper are three-fold:

1. We formulate a discrete approximation method in terms of a convex optimization of MMD in a reproducing kernel Hilbert space (RKHS), and solve it with the FW algorithm.
2. Our algorithm is computationally efficient and works well in high-dimensional problems. It guarantees a finite sample bound of the convergence rate which is in the linear order.
3. We gain not only theoretical improvements but also practical advances, including fast computation and a parallel algorithm that is theoretically assured.

2 Preliminary

In this section, we introduce discrepancy measures for evaluating the discrete approximation and reviews two existing methods, SVGD and SP.

2.1 Discrepancy measures

We start from the introduction of discrepancy measures, especially the worst case estimation error. Let $k : X \times X \rightarrow \mathcal{R}$ be the reproducing kernel of an RKHS \mathcal{H} of functions $\mathcal{X} \rightarrow \mathcal{R}$ with the inner product $\langle \cdot, \cdot \rangle$. MMD [13] is defined as $\text{MMD}(\{x_i\}_{i=1}^N)^2 = \sup_{f \in \mathcal{H}: \|f\|_{\mathcal{H}}=1} |Z_{f,p} - \frac{1}{N} \sum_{i=1}^N f(x_i)|^2 = \|\mu_p - \frac{1}{N} \sum_{i=1}^N k(x_i, \cdot)\|_{\mathcal{H}}^2$, where $\mu_p = \int k(\cdot, x)p(x)dx \in \mathcal{H}$. We can explicitly calculate this by

$$\text{MMD}(\{x_i\}_{i=1}^N)^2 = \iint k(x, x')p(x)p(x')dxdx' - 2\frac{1}{N} \sum_{n=1}^N \int k(x, x_n)p(x)dx + \frac{1}{N^2} \sum_{n,m=1}^N k(x_n, x_m).$$

Although MMD is suitable for two sample tests, it is difficult to use when $p(x)$ is an unnormalized distribution or a posterior distribution. In such a case, Stein discrepancy [25] is suitable. \mathcal{S}_p is denoted as the Stein operator, $\mathcal{S}_p\phi(x) = \nabla_x \ln p(x)\phi(x)^\top + \nabla_x \phi(x)$ and this satisfies $\mathbb{E}_p[\mathcal{S}_p\phi] = 0$. Stein discrepancy is defined by $\mathcal{S}(q\|p) = \sup_{f \in \mathcal{H}: \|f\|_{\mathcal{H}}=1} \mathbb{E}_q[\mathcal{S}_p\phi]$. It has been shown that Stein discrepancy can be expressed by $\mathcal{S}(q\|p) = \sqrt{\mathbb{E}_{x,y \sim q} k_s(x, y)}$, where $k_s(x, y) = \nabla_x \nabla_y k(x, y) + \nabla_x k(x, y) \nabla_y \ln p(y) + \nabla_y k(x, y) \nabla_x \ln p(x) + k(x, y) \nabla_x \ln p(x) \nabla_y \ln p(y)$, which is called the Stein reproducing kernel. When q is given by a discrete approximation \hat{p} , kernelized Stein discrepancy (KSD) can be written as $\mathcal{S}(\hat{p}\|p) = \sqrt{\sum_{i,j=1}^N k_s(x_i, x_j)}$. Both MMD and KSD are proper distances because $\hat{p} = p \Leftrightarrow \mathcal{S}(\hat{p}\|p) = 0$.

2.2 Stein variational gradient descent (SVGD)

In SVGD, we first prepare initial particles and iteratively update them by a transformation, $T(x) = x + \epsilon\phi(x)$, where $\phi(x)$ is a perturbation direction which is chosen to maximally decrease the Kullback-Leibler (KL) divergence between the empirical distribution formed by the particles and the target distribution, $\phi^*(x) = \arg \max_{\phi \in \mathcal{F}} \{-\frac{d}{d\epsilon} \text{KL}(q_{[\epsilon\phi]}\|p)|_{\epsilon=0}\}$,

where \mathcal{F} is a set of candidate functions from which we choose map ϕ . [26] proved that this problem is characterized by the Stein operator, $-\frac{d}{d\epsilon} \text{KL}(q_{[\epsilon\phi]}\|p)|_{\epsilon=0} = \mathbb{E}_{x \sim q}[\mathcal{S}_p\phi(x)]$. Thus, the optimization problem is $\mathcal{S}(q\|p) = \max_{\phi \in \mathcal{F}} \{\mathbb{E}_{x \sim q}[\mathcal{S}_p\phi(x)]\}$. The problem is how to choose an appropriate \mathcal{F} and when \mathcal{F} is the unit ball in an RKHS with kernel k , the optimal map is expressed by a kernelized Stein operator, $\phi^*(\cdot) = \mathbb{E}_{x \sim q}[\nabla_x \ln p(x)k(x, \cdot) + \nabla_x k(x, \cdot)]$. We approximate the expectation by the empirical approximation with $\{x_n^l\}_{n=1}^N$ and iteratively update particles. Theoretical analysis has been conducted in terms of the gradient flow and has shown convergence to the true target distribution asymptotically [23]. However, no finite sample bound has been established.

2.3 Stein points

SP [8] directly minimizes KSD. To obtain the n -th particle, we solve $\arg \min_x \sum_{i=1}^{n-1} k_s(x_i, x)$ or $\arg \min_x \sum_{i=1}^{n-1} k_s(x_i, x) + k_s(x, x)/2$. To solve these problems, authors [8] proposed using sampling methods or grid search. However, those methods are not applicable to high-dimensional problems due to the curse of dimensionality. Although an alternative way is to use gradient descent, this is computationally difficult in high-dimensional problems since this method needs to calculate a Hessian at each iteration. Moreover, the computational cost for evaluating the derivative of the log

probability is 4 times compared to SVGD. The advantage of this method is that a finite sample bound is available which converges in $\mathcal{O}(\sqrt{\log N/N})$.

3 Proposed methods

In this section, we formally develop our FWSS. We will introduce the FW algorithm in RKHS, propose our FWSS, and give a finite sample bound of our method.

3.1 Frank-Wolfe Stein sampling

On the basis of the existing methods reviewed in Section 2, we would like to obtain a method of approximating the posterior by discrete particles, which is computationally cheap and theoretically guaranteed. Our idea is to perform discrete approximation by minimizing MMD, instead of kernelized Stein discrepancy since it causes computational problems as we mentioned in the previous section. We minimize MMD, $J(\mu_{\hat{p}}) = \frac{1}{2} \|\mu_p - \mu_{\hat{p}}\|_{\mathcal{H}}^2$, in a greedy way. Since this is a convex function in an RKHS, we can use the FW algorithm.

The FW algorithm, also known as the conditional gradient method[17], is a convex optimization method. It focuses on the problem $\min_{x \in D} f(x)$, where f is a convex and continuous differentiable function. The procedure of the FW algorithm is shown in Alg. 1. Step 3 of the inner loop in Alg. 1 is often called the linear minimization oracle (LMO). As shown in Alg. 1, the FW algorithm optimizes the objective in a greedy way.

Algorithm 1: Frank-Wolfe (FW) Algorithm

```

1: Let  $\mathbf{x}_0 \in D$ 
2: for  $n = 0 \dots N$  do
3:   Compute  $\mathbf{s} = \operatorname{argmin}_{\mathbf{s} \in D} \langle \mathbf{s}, \nabla f(\mathbf{x}_n) \rangle$ 
4:   Constant step:  $\lambda_n = \frac{1}{n+1}$ 
5:   [Line search:  $\lambda_n = \operatorname{argmin}_{\lambda \in [0,1]} f((1-\lambda)\mathbf{x}_n + \lambda\mathbf{s})$ ]
6:   Update  $\mathbf{x}_{n+1} = (1-\lambda_n)\mathbf{x}_n + \lambda_n\mathbf{s}$ 
7: end for

```

In [1, 7], the equivalence of kernel herding [9] and the FW algorithm for MMD was clarified. In our situation, we minimize MMD on the marginal polytope \mathcal{M} of the RKHS \mathcal{H} , which is defined as the closure of the convex hull of $k(\cdot, x)$. We also assume that all data are uniformly bounded in the RKHS, i.e., for any data x , $\exists R > 0 : \|k(\cdot, x)\|_{\mathcal{H}} \leq R$.

The LMO calculation becomes $\arg \min_{g \in \mathcal{M}} \langle \mu_{\hat{p}}^{(n)} - \mu_p, g \rangle$. Actually, the minimizer of a linear function in a convex set is the extreme points of the domain, and thus we derive

$$\arg \min_{g \in \mathcal{M}} \langle \mu_{\hat{p}}^{(n)} - \mu_p, g \rangle = \arg \min_x \langle \mu_{\hat{p}}^{(n)} - \mu_p, k(\cdot, x) \rangle = \arg \min_x \sum_{l=0}^n w_l^{(n)} k(x_l, x) - \mu_p(x), \quad (2)$$

where $\mu_p(x) = \int k(x', x)p(x)dx$ and $w_l^{(n)}$ denotes the weights of the particle at the n -th iteration which is calculated by the step size. We solve this LMO by gradient descent. Since the objective of LMO is non-convex, we cannot obtain a global optimum by gradient descent in general. Fortunately, even if we solve LMO approximately, FW enables us to establish a theoretical finite sample bound [17, 21, 20, 28]. In such an approximate LMO, we set the accuracy parameter $\delta \in (0, 1]$ and consider the following problem instead of the original strict LMO:

$$\langle \mu_{\hat{p}}^{(n)} - \mu_p, \tilde{g} \rangle = \delta \min_{g \in \mathcal{M}} \langle \mu_{\hat{p}}^{(n)} - \mu_p, g \rangle. \quad (3)$$

This is much easier to solve than the original strict LMO. We call this step Approx-LMO. Thus, we can rely on the gradient descent to solve Approx-LMO. The derivative with respect to x when we use the symmetric kernel k can be written as follows:

$$\nabla_x \text{MMD}(x)^2 := \nabla_x \langle \mu_{\hat{p}}^{(n)} - \mu_p, g \rangle = \frac{1}{n} \sum_{l=0}^n w_l^{(n)} \nabla_x k(x_l, x) + \frac{1}{n} \sum_{l=0}^n w_l^{(n)} k(x, x_l) \nabla_{x_l} \ln p(x_l). \quad (4)$$

The proof is given in Appendix A. This is obtained by Stein's identity and empirical approximations with already processed particles. We can use the information of the derivative of the score function, $\nabla_x \ln p(x)$. The derivative information is very useful for the high-dimensional problems, so our algorithm is applicable to high-dimensional problems. On the basis of this Approx-LMO, we can consider Alg. 2 and Alg. 3, which greedily increase the particles following the FW framework to minimize MMD. For FW, we have to specify the initial state $\mu_{\hat{p}}^{(0)}$ and the step size of the algorithm. We consider two methods for specifying them. The first one is to specify the initial point randomly as drawn from the prior distribution. Since the particles obtained in early steps in this approach are not reliable, in each update, we have to reduce their importance gradually by using the constant step or line search. The weights of early particles decrease as the algorithm proceeds.

The second method is preparing the initial state by MAP estimation. In this approach, we cannot use the constant step or line search since early particles are located in highest probability mass regions. Therefore, we set the step size by the same way as the fully corrective Frank-Wolfe [20]. In all of the experiments, we use the fully corrective variant. Actually, the optimal weights can be calculated by using the Bayesian quadrature weight [16], $w_{\text{BQ}}^{(n)} = \sum_m z_j^\top K_{nm}^{-1}$, where K is the Gram matrix, $z_n = \int k(x, x_n) p(x) dx$, and we approximate the integral with particles. In Alg. 3, we only showed the fully corrective version of our proposed methods. The constant step and line search versions are shown in Appendix B.

Algorithm 2: Approx-LMO

```

1: Input:  $\mu_{\hat{p}}^{(n)}$ 
2: Output:  $k(\cdot, x^{L+1})$ 
3: for  $l = 0 \dots L$  do
4:   Compute  $\nabla_x \text{MMD}(x)^2$  by Eq.(4)
5:   Update  $x^{(l+1)} \leftarrow x^{(l)} + \epsilon^{(l)} \cdot \nabla_x \text{MMD}(x)^2$ 
6: end for

```

Algorithm 3: Frank Wolfe Stein Sampling (FWSS)

```

1: Input: A target density  $p(x)$ 
2: Calculate MAP estimation for  $\mu_{\hat{p}}^{(0)}$ 
3: for iteration  $n$  do
4:    $\bar{g}_n = \text{Approx-LMO}(\mu_{\hat{p}}^{(n)})$ 
5:   Update  $\mu_{\hat{p}}^{(n+1)} = \text{Fully Correction}(\bar{g}_n, \mu_{\hat{p}}^{(n)})$ 
6: end for

```

Since the particles obtained by our algorithm have weights which may be different from $1/N$, we express the discrete approximation as $\hat{p}(x) = \sum_{n=1}^N w_n \delta(x - x_n)$ and the approximation of the expectation as $Z_{f,\hat{p}} = \sum_{n=1}^N w_n f(x_n)$. Based on this notation, our algorithm has the following properties:

Theorem 1 (Consistency) *The approximate posterior mean by Alg. 3 converges to the true integral $Z_{f,p}$ at the following rate:*

$$|Z_{f,p} - Z_{f,\hat{p}}| \leq \text{MMD}(\{(x_n)\}_{n=1}^N) \leq \sqrt{2d} e^{-\frac{R^2 \delta^2 N}{2d^2}}, \quad (5)$$

where d is the diameter of the marginal polytope \mathcal{M} , δ is the accuracy parameter, and R is the radius of the smallest ball of center μ_p included \mathcal{M} .

Note that the above proof can be found in Appendix C. Moreover, based on the Bayesian quadrature, we can regard $Z_{f,\hat{p}}$ as the posterior distribution of the Gaussian process [16] (see Appendix K for details) and assure the posterior contraction rate [7]. In our algorithm, this is achieved by reweighting the particles which are obtained by Alg. 3 with the Bayesian quadrature weights. Then,

Theorem 2 (Contraction) *Let $S \subseteq \mathbb{R}$ be an open neighborhood of the true integral $Z_{f,p}$ and let $\gamma = \inf_{r \in S^c} |r - Z_{f,p}| > 0$. Then the posterior probability of mass on $S^c = \mathbb{R} \setminus S$ vanishes at the following rate:*

$$\text{prob}(S^c) \leq \frac{2d}{\sqrt{\pi}\gamma} e^{-\frac{R^2 \delta^2 N}{2d^2} - \frac{\gamma^2}{4d^2} e^{\frac{R^2 N}{d^2}}}, \quad (6)$$

where d is the diameter of the marginal polytope \mathcal{M} , δ is the accuracy parameter and R is the radius of the smallest ball of center μ_p included \mathcal{M} .

The above proof can be found in Appendix D. Here, R depends on the choice of the kernel we use. We discuss the kernel choice in Appendix E. A theory for the constant step and line search is shown in Appendix B.

3.2 Parallel variant of FWSS

In FWSS, we can adapt a more practically useful variant of FW to our problem setting. When we consider high-dimensional problems, SP does not work. The computational costs per iteration of SVGD and FWSS are $\mathcal{O}(D^2 N^2)$ and $\mathcal{O}(D^2 N)$ when the computational costs of $\nabla \ln p(x)$ is $\mathcal{O}(D^2)$, where D is the dimension of the target density. For a high-dimensional problem, we need a huge number of particles to approximate the high-dimensional target density $p(x)$. For these reasons, SVGD and FWSS are difficult to apply. To overcome this limitation due to the high-dimensionality, we use a variant of the FW algorithm, the asynchronous parallel block-coordinate FW (AP-BCFW) algorithm [30]. An advantage of AP-BCFW is that we can optimize the block separable domain problem in parallel. The problem, $\min_x f(x)$ s.t. $x = [x_1, \dots, x_d] \in \times_{i=1}^d \mathcal{M}_i$ can be broken into d independent sub-LMO problems, $\min_{s_i \in \mathcal{M}_i} \langle s_i, \nabla_i f(x) \rangle$.

In our problem setting, when we use specific kernels, we can factorize the kernel as, $k(x, y) = \prod_{i=1}^D k(x_{(i)}, y_{(i)})$. This means that our problem is $J(\mu_p) = \frac{1}{2} \|\mu_p - \mu_{\hat{p}}\|_{\mathcal{H}}^2$, $\mathcal{H} = \times_{i=1}^D \mathcal{H}_i$. Based on this factorization, we propose parallel block coordinate FWSS (PBC-FWSS) given in Alg. 4. In the algorithm, each worker calculates $\bar{g}_{n(i)} = k(x_{(i)}, \cdot)$, which corresponds to deriving the i -th dimension of a particle. A detailed explanation is given in Appendix F.

Algorithm 4: Parallel Block Coordinate FWSS (PBC-FWSS)

- 1: **Input:** A target density $p(x)$, a set of workers \mathcal{O} .
- 2: Calculate MAP estimation for $\mu_p^{(0)}$
- 3: Broadcast $\mu_p^{(0)}$ to all workers in \mathcal{O}
- 4: **for** iteration n **do**
- 5: Each oracle calculate $\bar{g}_{n(i)} = \text{Approx} - \text{LMO}(\mu_p^{(n)})|_{i=1}^D$
- 6: Keep reserving $(i, \bar{g}_{n(i)})$ from \mathcal{O}
- 7: Update $\mu_p^{(n+1)} = \text{Fully Correction}(\otimes_i^D \bar{g}_{n(i)}, \mu_p^{(n)})$
- 8: Broadcast $\mu_p^{(n+1)}$ to \mathcal{O} .
- 9: **end for**

This proposed algorithm converges sublinearly or linearly depending on the step width, which is discussed in Appendix F. The computational cost per iteration per worker in APBC-FWSS is $\mathcal{O}(d^2 N)$, where d is the number of dimensions assigned to each worker, which is $d \leq D$.

4 Discussion

In this section, we discuss the relationship between our method and SVGD, SP, variational boosting, and quasi Monte Carlo.

4.1 Relation to SVGD

SVGD is the method of optimizing a fixed number of particles simultaneously. On the other hand, FWSS is the greedy method adding new particles one per step. Both methods work well in high-dimensional problems. To approximate the high dimensional target distribution, we need many particles, but it is unclear how many particles are needed beforehand. Thus, greedy approach is preferable for the high-dimensional problems. Since in SVGD it is unclear how we can increase the number of particles after we finish the optimization, FWSS is better in such a case. However, simultaneous optimization is sometimes efficient and show better performance compared to a greedy approach. Based on this fact, we combine SVGD and FWSS by focusing on the fact that the update equations of SVGD and FWSS are

almost the same except for the weights. More specifically, we prepare particles by SVGD first, and then apply FWSS by treating particles obtained by SVGD as the initial state of each greedy particle. For details, please see Appendix I. This combination enables us to enjoy the efficient simultaneous optimization of SVGD and the greedy property and theoretical guarantee of FWSS.

In terms of computational cost, SVGD is $O(N^2)$ per iteration. In FWSS, we only optimize one particle, thus, its computational cost is $O(N)$. Up to N -th particle, the total cost is $O(N(N+1)/2)$, which is in the same order as SVGD. However, the number of LMO iterations in FWSS is much smaller than that of SVGD since the problem handles only one particle in FWSS, which is much easier than SVGD which treats N particles simultaneously. Therefore, we can expect the computational cost of FWSS to be cheaper than SVGD.

4.2 Relation to SP

The biggest difference between FWSS and SP is the objective function. Due to this difference, we use gradient descent to obtain new particles which are still effective in high-dimensional problems. However, SP minimizes KSD, so we cannot use gradient descent since the calculation requires evaluations of the Hessian at each step, which is impossible in high-dimensional problems. To cope with this problem, SP use sampling or grid search for optimization, which does not work in high-dimensional problems due to the curse of dimensionality.

Another difference is that we use FW to establish a greedy algorithm. This enables us to utilize many useful variants of the FW algorithm including the distributed variant explained in the previous section. In addition to the distributed variants of the FW algorithm, we can reduce the computational cost by utilizing the lazy FW framework [6]. We propose Algorithm 10 which is shown in Appendix J.

However, compared with SP, we cannot evaluate the objective function directly, so we have to use other performance measures such as the log likelihood, accuracy, or RMSE in test datasets. For SP, we can directly evaluate KSD at each iteration.

4.3 Relation to variational boosting

The proposed method is closely related to variational boosting [27]. In [27], the authors analyzed the variational boosting by using the FW algorithm and showed the convergence to the target distribution. In variational boosting, we use a mixture of Gaussian distributions as an approximate posterior and increase its flexibility by increasing the number of components in the mixture of Gaussian distributions. The intuition behind the convergence of variational boosting is that any distribution can be expressed by appropriately combining Gaussian mixture distributions. That situation is quite similar to FWSS, where we increase the number of particles greedily. In FWSS, we can regard each particle as corresponding to each component of variational boosting. In both methods, the flexibility of the approximate posterior grows as we increase the number of components or particles and this shows the linear convergence under certain conditions. The difference is that we consider the solution in an RKHS and minimize MMD to approximate the posterior for FWSS, variational boosting minimizes the KL divergence and treats it in the parameter space.

4.4 Relation to quasi Monte Carlo

If $p(x)$ is a prior distribution, quasi Monte Carlo methods, such as kernel herding [9] or Bayesian quadrature [12], are useful. In quasi Monte Carlo, we decide x_n s to directly minimize some criterions. For example, in the kernel herding method [9, 1], the discrepancy measure is MMD. Actually, we can coordinate the weights of each particle, $\hat{Z}_{f,p} = \sum_{n=1}^N w_n f(x_n)$ and this weight is set to be $1/N$ in SVGD or Monte Carlo. The kernel herding algorithm minimizes MMD in a greedy way. Since we assume that we have many particles from $p(x)$ and that we only choose the best particle that satisfies the above expression. In FWSS, we cannot prepare the particles beforehand, and thus, we directly derive particles by gradient descent. Another example of quasi Monte Carlo is Bayesian quadrature [12, 16], where we put the Gaussian process prior to f with kernel k and mean 0 (for details please see Appendix K). These kinds of quadrature rules are widely used and combined with some Stein methods, e.g., [24, 15].

Table 2: Benchmark results on test RMSE and log likelihood by Bayesian neural net regression model

Dataset	Posterior dimension	Avg. Test RMSE		Avg. Test log likelihood		Fixed Wall clock Time (Secs)
		SVGD	Ours	SVGD	Ours	
Naval (N=11,934, D=17)	953	4.9e-4±7.5e-5	4.2e-4±5.3e-5	6.08 ± 0.11	6.00±0.12	150
Protein (N=45730, D=9)	553	4.51 ± 0.057	4.43±0.035	-2.93 ± 0.013	-2.91±0.0073	40
Year (N=515344, D=91)	9203	9.54 ± 0.08	9.50±0.09	-3.65±0.005	-3.65±0.011	300

Other related work

Recently, there has been a tendency to combine an approximation of the posterior with optimization methods, which assures us of some theoretical guarantee. For example, variational boosting [27, 10], which performs the variational inference by mirror descent, have been studied so far. Our approach also performs the discrete approximation by convex optimization in an RKHS. The FW approach for sampling has already been shown to be successful, e.g., in [22].

5 Numerical experiments

We experimentally confirmed the usefulness of the proposed method compared with SVGD in both toy datasets and real world datasets. In all experiments, we used the radial basis function kernel, $k(x, x') = \exp(-\frac{1}{2h^2}|x - x'|^2)$, where h is the kernel bandwidth. The choice of h is critical to the success of the algorithms. There are three methods to specify the bandwidth, fixed bandwidth, median trick, gradient descent. We experimented on the above three choices and found that a fixed kernel bandwidth and the median trick are stable in general, and thus, we only show the results obtained by the median trick in this section. The results of other methods are shown with other detailed experimental settings in Appendix G. However, choosing the bandwidth well is still an open problem to be solved. For the approx-LMO, we used Adam [19] for all experiments. About the benchmark experiment, we split dataset 90% for training and 10% for testing. Due to space limitations, the toy data results are shown in Appendix G.

The first purpose of the experiments is to confirm that our algorithm is faster than SVGD in terms of wall clock time. This is because, as mentioned in Section 4.1, it solves simple problems compared with SVGD, thus we need less number of iterations to optimize each particle than that of SVGD. The second purpose is to confirm whether our algorithm converges linearly. Due to space limitations, we show only the results for FWSS and SVGD. The results for PBC-FWSS and Stein points are shown in Appendix G.

Bayesian logistic regression

We considered Bayesian logistic regression for binary classification. The settings were the same as in those [26], where we put a Gaussian prior $p_0(w|\alpha) = N(0, \alpha^{-1})$ for regression weights w and $p_0(\alpha) = \text{Gamma}(1, 0.01)$. As the dataset, we used Covertypes [11], with 581,012 data points and 54 features. The posterior dimension is 56. The results are shown in Fig. 1. In Fig. 1(a), the vertical axis is the test accuracy and the horizontal axis is wall clock time. As we discussed in Section 4.1, our algorithm was faster than SVGD in terms of wall clock time. Our method was also faster than SVGD. Stein points did not work well. We also compared FWSS with stochastic gradient Langevin dynamics(SGLD) [31] and faster than SGLD. In Appendix G, we also studied the situation where the first particle does not correspond to MAP estimation, and instead random initialization. Fig. 1(b) shows the convergence behavior, where the vertical axis is MMD² and the horizontal one is the number of particles in log scale. To calculate MMD, we generated “true samples” by Hamiltonian Monte Carlo [29]. In the figure, the results for MAP initialization is shown and our proposed method linearly converged, which is consistent with our convergence theory. As discussed in [7], although we used RBF kernel, we can observe the linear convergence thanks to the rounding in computer (see Appendix E for details).

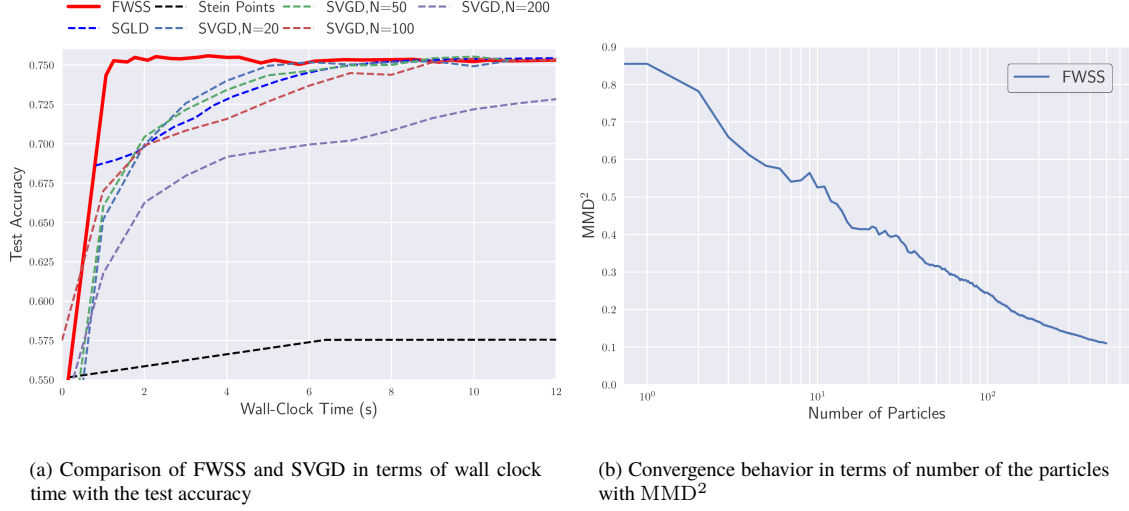


Figure 1: Comparison for the logistic regression model

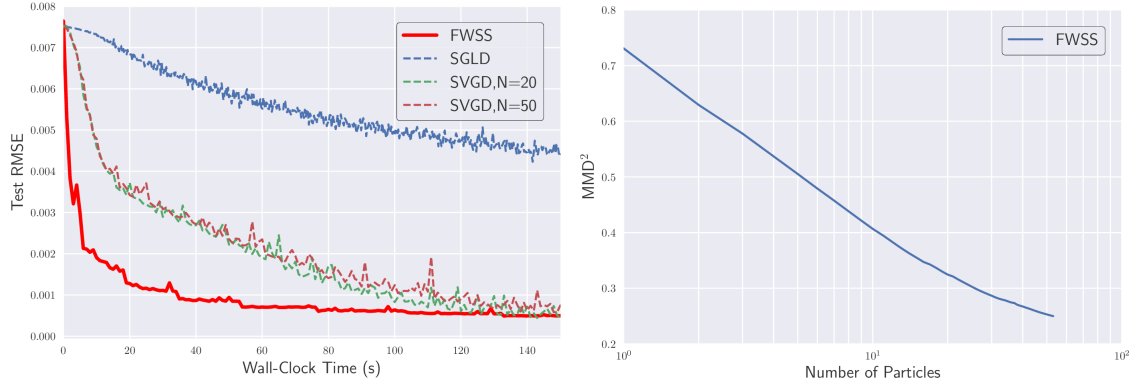
Bayesian neural net regression

We experimented with Bayesian neural networks for regression. The settings were the same as those in [26]. We used a neural network with one hidden layer, 50 units, and the ReLU activation function. As the dataset, we used the Naval data from the UCI [11], which contains 11,934 data points and 17 features. The posterior dimension was 953. The results are shown in Fig. 2. In Fig. 2(a), the vertical axis is the test RMSE, and the horizontal axis is wall clock time. In Fig 2(b), the vertical axis is the MMD^2 , and the horizontal axis is the number of particles. Since it is difficult to prepare MAP initialization for Bayesian neural networks at first in FWSS, we consider non-MAP initialization, and we gradually reduced earlier weight sizes by adjusting the step size. The posterior dimension was much higher than that of the logistic regression, but our algorithm was faster than SVGD in terms of wall clock time and linearly converged, which is consistent with the theory.

Results for other datasets are shown in Table 2, where we fixed the wall clock time and applied FWSS and SVGD within that period. We experimented 5 random trials for changing the splitting the dataset. For the Protein data, we used the same model as the Naval data, and for the Year data, we used the same model as others except that the number of hidden units is 100. From these benchmark dataset experiments, we confirmed that our method shows almost the same performance as SVGD in many cases but shows faster optimization. Moreover, it shows linear convergence.

6 Conclusions

In this work, we proposed FWSS which is an approximation method for integrating unnormalized distributions, especially posterior distributions. Compared with existing methods, our method is theoretically guaranteed and computational costs are cheap. In practice, our algorithm is faster than existing methods in terms of wall clock time and works well even in high-dimensional problems. Thanks to the Frank-Wolfe formulation, we can obtain not only a theoretical guarantee but also practical benefits, such as a parallel algorithm. As future work, we will further extend our method by combining other variants of the Frank-Wolfe algorithm or by applying our method to deep models.



(a) Comparison of FWSS and SVGD in terms of wall clock time with test RMSE

(b) Convergence behavior in terms of the number of the particles with MMD^2

Figure 2: Comparison for the Bayesian neural net regression model

References

- [1] Francis Bach, Simon Lacoste-Julien, and Guillaume Obozinski. On the equivalence between herding and conditional gradient algorithms. In *ICML 2012 International Conference on Machine Learning*, 2012.
- [2] Robert Bamler, Cheng Zhang, Manfred Opper, and Stephan Mandt. Perturbative black box variational inference. In *Advances in Neural Information Processing Systems*, pages 5086–5094, 2017.
- [3] Amir Beck and Marc Teboulle. A conditional gradient method with linear rate of convergence for solving convex linear systems. *Mathematical Methods of Operations Research*, 59(2):235–247, 2004.
- [4] Christopher M Bishop. *Pattern recognition and machine learning*. springer, 2006.
- [5] David M Blei, Alp Kucukelbir, and Jon D McAuliffe. Variational inference: A review for statisticians. *Journal of the American Statistical Association*, 112(518):859–877, 2017.
- [6] Gábor Braun, Sebastian Pokutta, and Daniel Zink. Lazifying conditional gradient algorithms. In *International Conference on Machine Learning*, pages 566–575, 2017.
- [7] François-Xavier Briol, Chris Oates, Mark Girolami, and Michael A Osborne. Frank-wolfe bayesian quadrature: Probabilistic integration with theoretical guarantees. In *Advances in Neural Information Processing Systems*, pages 1162–1170, 2015.
- [8] Wilson Ye Chen, Lester Mackey, Jackson Gorham, François-Xavier Briol, and Chris J Oates. Stein points. *arXiv preprint arXiv:1803.10161*, 2018.
- [9] Yutian Chen, Max Welling, and Alex Smola. Super-samples from kernel herding. In *Proceedings of the Twenty-Sixth Conference on Uncertainty in Artificial Intelligence*, pages 109–116. AUAI Press, 2010.
- [10] Bo Dai, Niao He, Hanjun Dai, and Le Song. Provable bayesian inference via particle mirror descent. In *Artificial Intelligence and Statistics*, pages 985–994, 2016.

- [11] Dua Dheeru and Efi Karra Taniskidou. UCI machine learning repository, 2017.
- [12] Zoubin Ghahramani and Carl E Rasmussen. Bayesian monte carlo. In *Advances in neural information processing systems*, pages 505–512, 2003.
- [13] Arthur Gretton, Karsten M Borgwardt, Malte J Rasch, Bernhard Schölkopf, and Alexander Smola. A kernel two-sample test. *Journal of Machine Learning Research*, 13(Mar):723–773, 2012.
- [14] Jacques Guélat and Patrice Marcotte. Some comments on wolfe’s Aaway step. *Mathematical Programming*, 35(1):110–119, 1986.
- [15] Jun Han and Qiang Liu. Stein variational adaptive importance sampling.
- [16] Ferenc Huszár and David Duvenaud. Optimally-weighted herding is bayesian quadrature. In *Proceedings of the Twenty-Eighth Conference on Uncertainty in Artificial Intelligence*, pages 377–386. AUAI Press, 2012.
- [17] Martin Jaggi. Revisiting frank-wolfe: Projection-free sparse convex optimization. In *ICML (1)*, pages 427–435, 2013.
- [18] Wittawat Jitkrittum, Wenkai Xu, Zoltán Szabó, Kenji Fukumizu, and Arthur Gretton. A linear-time kernel goodness-of-fit test. In *Advances in Neural Information Processing Systems*, pages 261–270, 2017.
- [19] Diederik P Kingma and Jimmy Ba. Adam: A method for stochastic optimization. *arXiv preprint arXiv:1412.6980*, 2014.
- [20] Simon Lacoste-Julien and Martin Jaggi. On the global linear convergence of frank-wolfe optimization variants. In *Advances in Neural Information Processing Systems*, pages 496–504, 2015.
- [21] Simon Lacoste-Julien, Martin Jaggi, Mark Schmidt, and Patrick Pletscher. Block-coordinate frank-wolfe optimization for structural svms. In *International Conference on Machine Learning*, pages 53–61, 2013.
- [22] Simon Lacoste-Julien, Fredrik Lindsten, and Francis Bach. Sequential kernel herding: Frank-wolfe optimization for particle filtering. *arXiv preprint arXiv:1501.02056*, 2015.
- [23] Qiang Liu. Stein variational gradient descent as gradient flow. In *Advances in neural information processing systems*, pages 3118–3126, 2017.
- [24] Qiang Liu and Jason Lee. Black-box importance sampling. In *Artificial Intelligence and Statistics*, pages 952–961, 2017.
- [25] Qiang Liu, Jason Lee, and Michael Jordan. A kernelized stein discrepancy for goodness-of-fit tests. In *International Conference on Machine Learning*, pages 276–284, 2016.
- [26] Qiang Liu and Dilin Wang. Stein variational gradient descent: A general purpose bayesian inference algorithm. In *Advances In Neural Information Processing Systems*, pages 2378–2386, 2016.
- [27] Francesco Locatello, Rajiv Khanna, Joydeep Ghosh, and Gunnar Rätsch. Boosting variational inference: an optimization perspective. *arXiv preprint arXiv:1708.01733*, 2017.
- [28] Francesco Locatello, Rajiv Khanna, Michael Tschannen, and Martin Jaggi. A unified optimization view on generalized matching pursuit and frank-wolfe. In *Proceedings of the 20th International Conference on Artificial Intelligence and Statistics*, number EPFL-CONF-229229, 2017.

- [29] Radford M Neal et al. Mcmc using hamiltonian dynamics. *Handbook of Markov Chain Monte Carlo*, 2(11), 2011.
- [30] Yu-Xiang Wang, Veeranjanyulu Sadhanala, Wei Dai, Willie Neiswanger, Suvrit Sra, and Eric Xing. Parallel and distributed block-coordinate frank-wolfe algorithms. In *International Conference on Machine Learning*, pages 1548–1557, 2016.
- [31] Max Welling and Yee W Teh. Bayesian learning via stochastic gradient langevin dynamics. In *Proceedings of the 28th International Conference on Machine Learning (ICML-11)*, pages 681–688, 2011.

A Proof of Eq. (4)

For the symmetric kernel k , the relation $\nabla_x k(x - y) = \nabla_y k(x - y)$ holds, and we apply the partial integral method to the first term, then

$$\begin{aligned} \nabla_{x_n} \int k(x, x_n) p(x) dx &= \int \nabla_{x_n} k(x, x_n) p(x) dx = \int \{\nabla_x k(x, x_n)\} p(x) dx \\ &= k(x, x_n) p(x) \Big|_{-\infty}^{\infty} - \int k(x, x_n) \nabla_x p(x) dx = -\mathbb{E}_{p(x)} [k(x, x_n) \nabla_x \ln p(x)] \end{aligned} \quad (7)$$

This is also obtained by Stein’s identity.

To approximate the integral, we usually use importance sampling when the analytic form of the integral is not available. Here, FWSS is the greedy approach, therefore we have particles which had already been processed. Thus we approximate the expectation by the empirical distributions which is composed by processed particles. The FW framework does not need the exact solution of LMO. We just approximately solve it. At the early stage of the algorithm, there are not so many particles and those particles are not so reliable, hence the expectation is not so reliable. Fortunately, they are enough to solve the LMO approximately. And as the algorithm proceeds, the weights of those early unreliable particles are gradually reduced by the step size. Thus, we solve the LMO by the gradient which is written by

$$\nabla_{x_n} \int k(x, x_n) p(x) dx \simeq -\frac{1}{N} \sum_{m=1}^N k(x_m, x_n) \nabla_{x_m} \ln p(x_m). \quad (8)$$

Thus, we can obtain the update equation,

$$\nabla_x \text{MMD}(x)^2 := \nabla_x \langle \mu_{\hat{p}}^{(n)} - \mu_p, g \rangle = \frac{1}{n} \sum_{l=0}^n w_l^{(n)} \nabla_x k(x_l, x) + \frac{1}{n} \sum_{l=0}^n w_l^{(n)} k(x, x_l) \nabla_{x_l} \ln p(x_l). \quad (9)$$

In the above expression, the first term corresponds to the regularization term, which try to scatter the particles. When we use the RBF kernel, the first term is proportional to the inverse of the bandwidth. Thus, it is easily understand that small bandwidth makes regularization term large, and vise versa. The second term try to move particles in high mass regions.

B Step size selection

Algorithm 5: Frank Wolfe Stein Sampling(FWSS)

```

1: Input: A target density  $p(x)$ 
2: Prepare initial particle  $\mu_{\hat{p}}^{(0)}$  (Prepare by randomly, sample from prior or MAP)
3: for iteration  $n$  do
4:    $\bar{g}_n = \text{Approx-LMO}(\mu_{\hat{p}}^{(n)})$ 
5:   if Constant step then
6:      $\lambda_n = \frac{1}{\gamma+1}$ 
7:     Update  $\mu_{\hat{p}}^{(n+1)} = (1 - \lambda_l)\mu_{\hat{p}}^{(n)} + \lambda_n \bar{g}_n$ 
8:   else if Line search: then
9:      $\lambda_n = \text{argmin}_{\lambda \in [0,1]} J((1 - \lambda)\mu_{\hat{p}}^{(n)} + \lambda \bar{g}_n)$ 
10:    Update  $\mu_{\hat{p}}^{(n+1)} = (1 - \lambda_l)\mu_{\hat{p}}^{(n)} + \lambda_n \bar{g}_n$ 
11:   else
12:     Update  $\mu_{\hat{p}}^{(n+1)} = \text{Fully Correction}(\bar{g}_n, \mu_{\hat{p}}^{(n)})$ 
13:   end if
14: end for

```

An appropriate step size is crucial for the success of the FW. Generally, there are three choices as shown in Alg 5. Common choices are the constant step size and Line search. The step size of line search can be written as

$$\lambda_n = \frac{\langle \mu_{\hat{p}}^{(n)} - \mu_p, \mu_{\hat{p}}^{(n)} - \bar{g}_{n-1} \rangle}{\|g_{i-1} - \bar{g}_n\|_{\mathcal{H}}^2}. \quad (10)$$

The point is that they gradually reduce the weights of earlier particles. Thus, those weights are preferable when the early particles are not reliable. In our algorithm, those weights are preferable when we cannot prepare the MAP initialization.

Another choice of the step size is the Fully correction. As the name means, this method updates the weights of all particles which have already been processed at each step. In our algorithm, we used the Bayesian Quadrature weights since they are the optimal weights for the MMD. For more details of the Bayesian Quadrature, please see the Appendix K. The weights can be calculated by

$$w_{\text{BQ}}^{(n)} = \sum_m z_j^\top K_{nm}^{-1}, \quad (11)$$

where K is the gram matrix, $z_n = \int k(x, x_n)p(x)dx$ and we approximate the integral by particles. Fully correction is preferable when the early particles are important. In our algorithm, this corresponds to the situation where we can successfully obtain the MAP initialization.

In Alg 5, we actually do not need the MAP initialization. because by choosing the appropriate step size, the weights of those unreliable particles will become small.

The step size choice effects the convergence rate directly. In the main text, we only showed the results of Fully correction. Here, we show the results of the constant step size and Line search.

Theorem 3 (Consistency) *The approximate posterior mean $\hat{Z}_{f,p}$ by Alg 5) converges to the true integral $Z_{f,p}$ at the following rates*

$$|Z_{f,p} - Z_{f,\hat{p}}| \leq \text{MMD}(\{(x_n)\}_{n=1}^N) \leq \begin{cases} \frac{2d^2}{R\delta N} & \text{for Constant step} \\ \sqrt{2}de^{-\frac{R^2\delta^2 N}{2d^2}} & \text{for Line search} \end{cases} \quad (12)$$

where d is the diameter of the marginal polytope \mathcal{M} , δ is the accuracy parameter, R is the radius of the smallest ball of center μ_p included \mathcal{M} .

Also, when we reweight the obtained particles by using Bayesian quadrature weights and interpret it as the posterior, the following contraction property holds,

Theorem 4 (Contraction) *Let $S \subseteq \mathbb{R}$ be an open neighborhood of the true integral $Z_{f,p}$ and let $\gamma = \inf_{r \in S^c} |r - Z_{f,p}| > 0$. Then the posterior probability of mass on $S^c = \mathbb{R} \setminus S$ by Alg 3) vanishes at a rate:*

$$\text{prob}(S^c) \leq \begin{cases} \frac{2\sqrt{2}d^2}{\sqrt{\pi}R\delta\gamma N} e^{-\frac{\gamma^2 R^2 \delta^2 N^2}{8d^4}} & \text{for Constant step} \\ \frac{2d}{\sqrt{\pi}\gamma} e^{-\frac{R^2 \delta^2 N}{2d^2} - \frac{\gamma^2}{4d^2} e^{\frac{R^2 N}{d^2}}} & \text{for Line search} \end{cases} \quad (13)$$

where d is the diameter of the marginal polytope \mathcal{M} , δ is the accuracy parameter, R is the radius of the smallest ball of center μ_p included \mathcal{M} .

C Proof of Theorem 5

First we consider the case of Line search variants. The proof goes almost in the same way as [3]. (The proof of [14] is also useful)

Here the notation is the same as [3] and we proof our theorem in the same way as Proposition 3.2. in [3]. We expand the Proposition 3.2 to the situation where we use the approximate LMO, where [3] consider the case of LMO. From Proposition 3.1 in [3], following relation holds.

$$\langle v_k, w_k \rangle \leq -R_s(\hat{x}, M) \|v_k\|. \quad (14)$$

We consider the approximate LMO whose accuracy parameter is δ . Approximate LMO returns \tilde{w} which deviates from the true w in the following way

$$\langle v_k, \tilde{w}_k \rangle \leq \delta \langle v_k, w_k \rangle. \quad (15)$$

From this definition, following holds

$$\langle v_k, \tilde{w}_k \rangle \leq -\delta R_s(\hat{x}, M) \|v_k\|. \quad (16)$$

Based on this expression, we replace the w_k by \tilde{w}_k in the proof of Proposition 3.2. in [3], and we obtain the variant of Eq.(12) in [3] which uses approximate LMO not LMO. After this, we use Eq.(16) for the evaluation of $\|v_k\|^2$ and we can obtain the following expression,

$$\|v_k\|^2 \leq \left(1 - \left(\frac{\delta R_s(\hat{x}, M)}{\|g\| + \rho_s \|M\|} \right)^2 \right) \|v_{k-1}\|^2 \quad (17)$$

From this expression, we can proof the linear convergence about v .

Based on this bound, we can apply the result of Ch.4.2 in [1].

Then, by utilizing the discussion of Appendix B in [7], we can obtain the following expression.

$$|Z_{f,p} - Z_{f,\hat{p}}| \leq \text{MMD}(\{x_i\}_{i=1}^N \|f\|_{\mathcal{H}} \leq \|\mu_p - \mu_{\hat{p}}\| \quad (18)$$

This is derived Cauchy Schwartz inequality and the definition of MMD and $\|f\|_{\mathcal{H}} \leq 1$. Thus, we have proved the theorem in the case of line search.

Fully corrective variants optimize all the weights, this is different from the line search that we derive the weight for one added particles. Hence

$$\|v_k^{\text{FC}}\|^2 \leq \|v_k\|^2 \leq \left(1 - \left(\frac{\delta R_s(\hat{x}, M)}{\|g\| + \rho_s \|M\|}\right)^2\right) \|v_{k-1}\|^2 \quad (19)$$

where v_k^{FC} is derived by fully corrective variants. Thus we can bound the fully corrective variant in the same expression as line search. Also, geometric convergence of fully correction variant is discussed in [27],[20]. They also discussed it by using the fact that fully correction is superior to line search.

Next we consider the constant step case. We prove our results based on Proposition 1 in [9]. The notation is the same as the in [9]. The sign of [9] is reverse to ours, e.g. Eq.(13). Thus we follow the [9] and we define the approximate LMO based on the Eq.(11) in [9], which can be written in the following way,

$$\langle w_t, \tilde{c}_k \rangle \geq \delta \langle w_t, c_k \rangle = \delta \max_{\mathbf{c}} \langle w_t, \mathbf{c} \rangle. \quad (20)$$

δ is the accuracy parameter and approximate LMO returns \tilde{c} . Combined with the above expression and Eq.(13) in [9], the following relation holds

$$\left\langle \frac{w_t}{\|w_t\|}, \frac{c_t}{\|c_t\|} \right\rangle \geq \delta \gamma^* \quad (21)$$

Based on this, $\|w\| \leq \frac{R}{\delta \gamma^*}$ holds. Following the same way as Eq.(14) in the Proposition 1 in [9], following relation holds,

$$\left\| \mu_p - \frac{1}{T} \sum_{t=1}^T \phi(\mathbf{x}_t) \right\| \leq \frac{\|w_0\| + \frac{R}{\delta \gamma^*}}{T} \quad (22)$$

This is the sub-linear convergence. In the above proof, we followed the expression of [9] and we use the normalized inner product γ^* . In the main paper, we do not normalize the inner product so we just replace the γ^* by $\gamma^*/\|c_t\| \geq \gamma^*/2R$.

In the above proof, we consider the fixed accuracy parameter δ for the approximate LMO. However the δ can be different at each approximate LMO calls. In that situation, we express the accuracy parameter of the k -th call as δ_k . We consider the worst accuracy LMO call and define $\delta = \min_k \delta_k$. About the Line search, if we put $\delta_k^2 q^2 = \left(\frac{R_s(\hat{x}, M)}{\|g\| + \rho_s \|M\|}\right)^2$, then following relation holds,

$$\|v_k\|^2 \leq \|v_0\|^2 e^{-q^2 \sum_{t=0}^k \delta_k} \leq \|v_0\|^2 e^{-q^2 k \min_k \delta_k} = \|v_0\|^2 e^{-q^2 k \delta} \quad (23)$$

About the constant step, following relation holds,

$$\left\langle \frac{w_t}{\|w_t\|}, \frac{c_t}{\|c_t\|} \right\rangle \geq \delta_k \gamma^* \geq \min_k \delta_k \gamma^* = \delta \gamma^*. \quad (24)$$

D Proof of Theorem 6

Our results are directly obtained by AppendixB of [7]. We use the proof of the contraction theorem. The calculations after Eq.(26) in [7] are hold in our case and Eq.(31) in [7] holds in our situation. Thus all we need to do is to substitute

the variance of ours into Eq.(31) in [7]. Our variance is derived by reweighting the particles obtained by FWSS with Bayesian Quadrature weight and calculate the weighted MMD. This is upper bounded by the bound of the result Theorem 5 because MMD which is calculated by Bayesian quadrature weight is the optimal. Thus, by substituting the result of Theorem 5 into Eq.(31) in [7], we obtain the result.

Actually, we cannot calculate the Bayesian Quadrature weight analytically, so we approximate it by obtained particles. Even in such a case, we can obtain the upper bound. The posterior distribution is denoted by $N(Z_{f,\hat{p}}, \sigma_N^2)$, where $\sigma_N = \text{MMD}(\{x_i, w_i^{\text{BQ}}\}_{i=1}^N)$, and w_i^{BQ} is the Bayesian Quadrature weight. Since we approximate this weight empirically and denote the corresponding variance by $\hat{\sigma}_N = \text{MMD}(\{x_i, \hat{w}_i^{\text{BQ}}\}_{i=1}^N)$. Since Bayesian Quadrature weight is the optimal weight, $\sigma_N \leq \hat{\sigma}_N$. Thus we can upper bound Eq.(31) in [7] by this variance whose weight is approximated by particles.

E Kernel selection

The choice of the kernel is crucial numerically and theoretically. In the above convergence proof, we assumed that within the affine hull \mathcal{M} , there exists a ball with center \hat{x} and radius R that is included in \mathcal{M} . [1, 7] proved that for infinite dimensional RKHS, such as the case of RBF kernel, this assumption never holds. Thus, we can only have the sub-linear convergence for RBF kernels in general. However, as pointed in [7], even if we use RBF kernels, thanks to the rounding in computer, what we treat in simulation are actually finite dimensional. This holds to our situation, and in the experiments we observe the linear convergence of our algorithm.

F APBC-FWSS

To apply the Asynchronous parallel block coordinate Frank Wolfe algorithm, the domain of the problem must be composed by the cartesian product and each component is convex hull, that is $\min_x f(x)$ s.t. $x = [x_1, \dots, x_d] \in \times_{i=1}^d \mathcal{M}_i$, each domain \mathcal{M}_i is convex. In our situation, the problem is $J(\mu_{\hat{p}}) = \frac{1}{2} \|\mu_p - \mu_{\hat{p}}\|_{\mathcal{H}}^2$, $\mathcal{H} = \times_{i=1}^d \mathcal{H}_i$, and the domain is the marginal polytope \mathcal{M} of the RKHS \mathcal{H} , which is defined as the closure of the convex hull of $k(\cdot, x)$. Thus we cannot directly apply the block coordinate algorithm to our setting. This can be easily confirmed in the following way. First we denote the convex hull in RKHS as $\sum_i \alpha_i k(x_i, \cdot) = \sum_i \alpha_i \phi_i$ where α_i is positive coefficient and this is expressed as

$$\sum_i \alpha_i \phi_i = \sum_i \alpha_i \otimes_d \phi_i^d, \quad (25)$$

where we assumed some special kernels that we can factorize it into cartesian product such as RBF kernels which satisfies $k(x, y) = \prod_{i=1}^d k(x_{(i)}, y_{(i)})$.

And to apply the block coordinate algorithm, each domain is the convex hull, that is,

$$\otimes_d \left(\sum_{i^d} \alpha_{i^d} \phi_{i^d} \right) = \sum_i \sum_j \sum_k \dots \alpha_i \alpha_j \alpha_k \dots (\phi_i \otimes \phi_j \otimes \phi_k \dots) \quad (26)$$

Thus, this is much larger space than our problem. To mediate this, we have to consider the synchronize algorithm not asynchronous one. That is if we can separate the our objective into each dimensions by using the cartesian product, we will solve the LMO in each dimension separately, and wait all the worker finish the each calculation. After that we combine all the results of the workers and update the $\mu_{\hat{p}}^{(n)}$. By using this strategy, in each LMO, we solve subproblems

in the convex hull, and can easily find the solution at the extreme points in each dimension, and synchronous update makes the particles in $\sum_i \alpha_i \otimes_d \phi_i^d$. The drawback of this strategy is that if some workers are slow, we have to wait them.

The next concern is whether we can separate our objective into each dimensions by using the cartesian product or not. In general, this is impossible since MMD entails the μ_p and

$$\mu_p = \mathbb{E}_{p(x)}[\otimes_d \phi(x_d)] = \int \otimes_d \phi(x_d) p(x_1, \dots, x_D) dx_1 \dots dx_D. \quad (27)$$

and this is not separable in general. However, we can separate them under conditional probability conditions which is a special case, when we focus on the update equation which we use to solve the LMO, and especially the derivative with respect to the d -th dimension of x ,

$$\begin{aligned} & \nabla_{x^{(d)}} \text{MMD}(x)^2 : \\ &= \nabla_{x^{(d)}} \langle \mu_{\hat{p}}^{(n)} - \mu_p, g \rangle \\ &= \frac{1}{n} \sum_{l=1}^n \nabla_{x^{(d)}} k(x_l, x) + \frac{1}{n} \sum_{l=1}^n k(x, x_l) \nabla_{x_l^{(d)}} \ln p(x_l) \\ &= \frac{1}{n} \sum_{l=1}^n \prod_{i \neq d} k(x_l^{(i)}, x^{(i)}) \left(\nabla_{x^{(d)}} k(x_l^{(d)}, x^{(d)}) + k(x_l^{(d)}, x^{(d)}) \nabla_{x_l} \ln p(x_l) \right) \end{aligned} \quad (28)$$

So, for d -th dimension, the effect of other dimensions comes from the coefficient $\prod_{i \neq d} k(x_l^{(i)}, x^{(i)})$. When we use an RBF kernel and optimize the particle, the change of the $\prod_{i \neq d} k(x_l^{(i)}, x^{(i)})$ is much smaller than the change inside the bracket. Thus we fix the value of $\prod_{i \neq d} k(x_l^{(i)}, x^{(i)})$ during the optimization. This enables us to separate the update of the particle in each dimension. This is especially useful when we use the median trick during the optimization, since the median trick tries to $\sum_j k(x_i, x_j) \sim N \exp(-\text{med}^2/h^2) = 1$ that is the sum of the coefficients of the gradients are coordinated to be 1. Hence the coefficient does not change so much during the iteration of the LMO. Based on this assumption, we can separately solve the LMO in each dimension, and the obtained particle satisfies the accuracy parameter in approximate LMO,

$$\langle \mu_{\hat{p}}^{(n)} - \mu_p, \tilde{g} \rangle = \delta \min_{g \in \mathcal{M}} \langle \mu_{\hat{p}}^{(n)} - \mu_p, g \rangle. \quad (29)$$

we can guarantee the algorithm in the same way as FWSS. We tested the algorithm on the benchmark dataset, and it seems work well. However the success of this algorithm depends on the above assumption and the validity of the assumption depends on the kernel and its hyperparameter. The RBF kernel and median trick seems satisfy the assumption and this is the reason that experiment works well.

G Details of Experiments

In this section, we show the detail experimental settings and results which we cannot show in the main paper due to the limit of the space.

G.1 Algorithm of SVGD

We implemented SVGD by following pseudo codes.

Algorithm 6: Stein Variational Gradient Descent

- 1: **Input:** A target density $p(x)$ and initial particles $\{x_n^0\}_{n=1}^N$
- 2: **Output:** Particles $\{x_i\}_{i=1}^n$ which approximate $p(x)$
- 3: **for** iteration l **do**
- 4: $x_n^{(l+1)} \leftarrow x_n^{(l)} + \epsilon^{(l)} \hat{\phi}^*(x_n^{(l)})$, where $\hat{\phi}^*(x) = \frac{1}{N} \sum_{n=1}^N \left[k(x_n^{(l)}, x) \nabla_{x_n^{(l)}} \ln p(x_n^{(l)}) + \nabla_{x_n^{(l)}} k(x_n^{(l)}, x) \right]$
- 5: **end for**

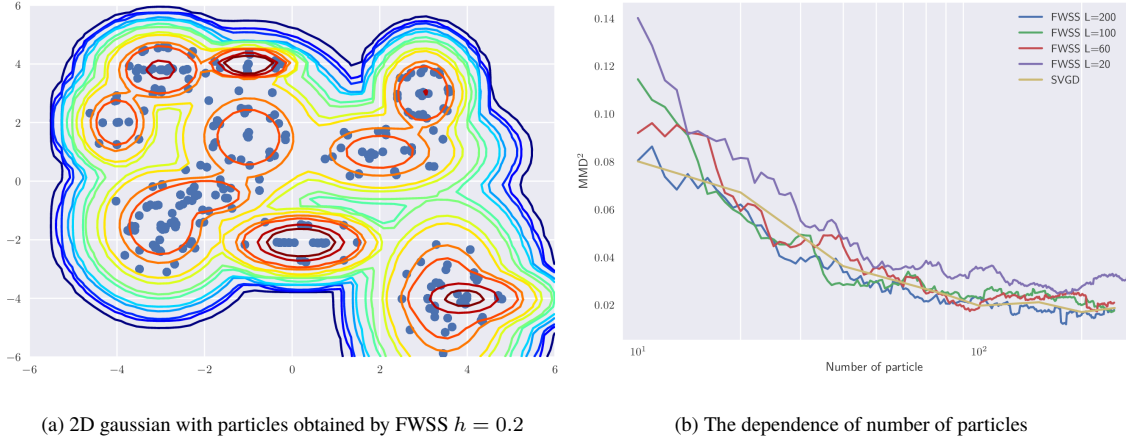


Figure 3: The results of the toy data by FWSS of fixed bandwidth

G.2 Toy dataset

To clarify how our method works, we checked our algorithm with a two dimensional toy dataset. The true distribution is a two dimensional mixture of Gaussians which is composed by 11 Gaussian distributions. Here we applied our FWSS and observed how the particles are fitted to the distribution. The results are shown in Fig 3. In this figure, the number of particle is 200 and $L = 50$ and $h = 0.3$. We also changed L , the number of gradient descent in the approx-LMO, and compared how MMD decreases with SVGD in Fig 3(b). We found that both our method and SVGD decrease linearly.

The selection of the bandwidth is crucial for the success of the method. As we had shown in the main paper, there are three ways to specify the bandwidth. The first choice is using the fixed bandwidth and this choice is often used in Bayesian quadrature, e.g., [7]. The second choice is the median trick which is used in SVGD [26]. This method enables us to choose the bandwidth adaptively during the optimization. The third choice is using the gradient descent for h to minimize the kernelized Stein discrepancy during optimization. This is used in [18].

In Fig 4, we showed other selection of bandwidth. As shown in Fig 4(a), the small bandwidth makes the particles sparsely scattered. This is due to the fact that the second term of the update equation, which corresponds to the regularization term becomes very large. Thus particles tend to take distance from each other. If we take a large bandwidth, the regularization term becomes small, and thus particles become close to each other which is shown in Fig 4(b).

Finally we showed the results of FWSS by median trick and SVGD, the result is shown in Fig. 5

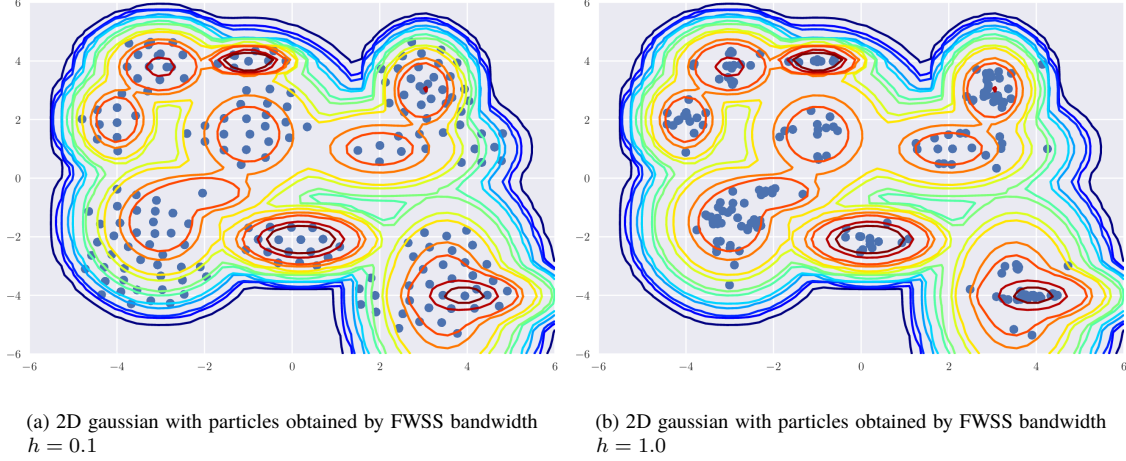


Figure 4: The results of the toy data by FWSS of fixed bandwidth

G.3 Details of the Benchmark experiments

Bayesian logistic regression

In this experiment, we used Adam with learning rate 0.005 and we split the data, 90% are used for training and 10% are used for test. Minibatch size is 100. For the LMO calculation, we set $L = 250$. We used the median trick for the kernel band width. To calculate the MMD, we have to fix the bandwidth of the kernel. We simply take the median of the bandwidth which changes adaptively during the optimization. In the main paper we used 2.5. To calculate the MMD, we generate samples by Hybrid Monte Carlo (HMC).

In the experiment of the main text, we first estimated the MAP state as the initial particles. Here we did the experiment that we made the initial particle randomly and continued our algorithm. The result is shown in Fig. 6, and corresponding random initial version is denoted by Non-MAP initialization in the figure. As you can see, although we did not use the MAP estimate, still our method is faster than SVGD.

Bayesian neural net regression

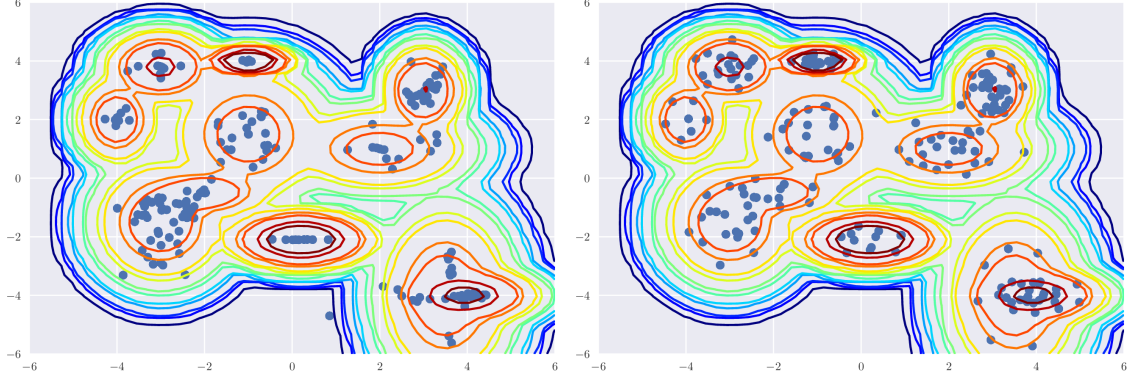
In this experiment, we used Adam with learning rate 0.005 and we split the data, 90% are used for training and 10% are used for test. minibatch size is 100 except for year dataset, where we used 500 minibatch size.

We use the zero mean Gaussian for the prior of the weights and we put $\text{Gamma}(1, 0.1)$ prior for the inverse covariances.

For the LMO calculation, we set $L = 1000$ except for year dataset where we set $L = 2000$. Since it is difficult to obtain the MAP estimation for the initial sates, this is corresponds to the case of Non-MAP initialization as we explained previous section.

In the main text, we showed the figure of naval dataset and here, we show that of the protein data in Fig. 7.

In the main paper, we checked the performance of FWSS and SVGD by fixing the computation time. Those fixed time are selected that the test RMSE are sufficiently converged.



(a) 2D gaussian with particles obtained by FWSS bandwidth by median trick

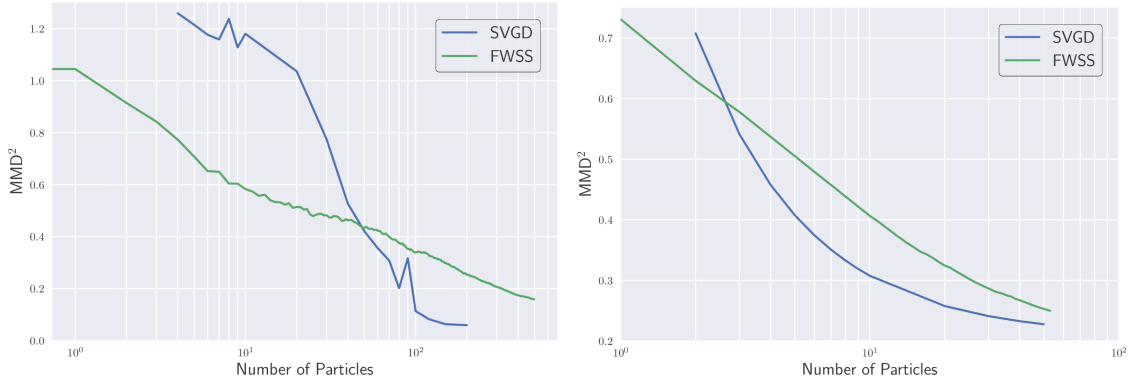
(b) 2D gaussian with particles obtained by SVGD

Figure 5: Boundaries of logistic regression using ordinary VI and the proposed method

G.4 MMD comparison between FWSS and SVGD

In the main paper, we only plot the result of FWSS about the MMD to confirm the linear convergence. Here we also plot the behavior of the MMD optimized by SVGD. We changed the number of particles and plot it. The value of MMD at each number of particles are calculated after the 30000 steps where the optimization had finished. The result is shown in Fig. 8.

To calculate the MMD, we also generate “true samples” by HMC. SVGD have smaller MMD compared to ours. This is due to the fact that SVGD simultaneously optimizes all particles and try to put particles in the best position which corresponds to the global optima. On the other hand, FWSS just increase the particles greedily and thus this results in a local optima. Hence the better performance of SVGD compared to FWSS at the same number of particles in terms of MMD is a natural result.



(a) MMD^2 comparison for Bayesian logistic regression

(b) MMD^2 comparison for Bayesian neural net regression

Figure 8: Comparison of MMD between FWSS and SVGD

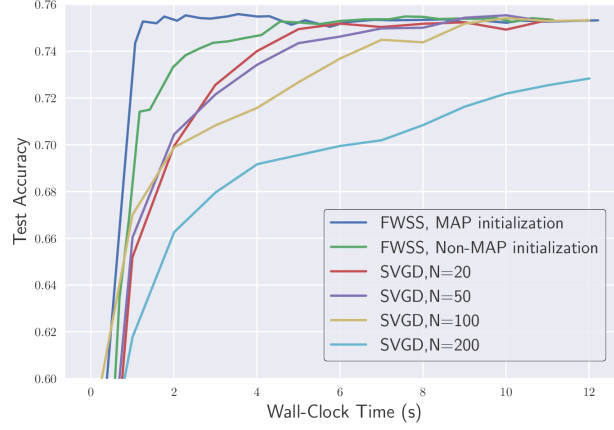


Figure 6: [Comparison of FWSS and SVGD in terms of wall clock time with test accuracy

G.5 Results of Other real dataset by PBC-FWSS

We did the comparison of PBC-FWSS, FWSS and SVGD for Bayesian neural net regression, where the model is one hidden layer with 100 units and Relu activation function. The data is Year dataset in UCI whose dataset size is 515344 and 91 features. The posterior dimension is 9203. We used minibatch size of 500 and optimize by Adam with 0.005 initial learning rate. For PBC-FWSS, we used 2 workers.

The results are shown in Fig 9. Those two figures are the same plot, where the left one is the enlargement of the right figure at early time.

As you can see that at early time, PBC-FWSS is the fastest. However as the optimization proceeds, the advantage of parallel computation had been disappeared. This might be due to our implementation in tensorflow that, for the parallel computation, we first separate the dimensions into each workers, this corresponds to the allocation of variables in tensorflow. Since this allocation makes the computation graph inefficient, and thus we did not gain so much speed up by PBC-FWSS.

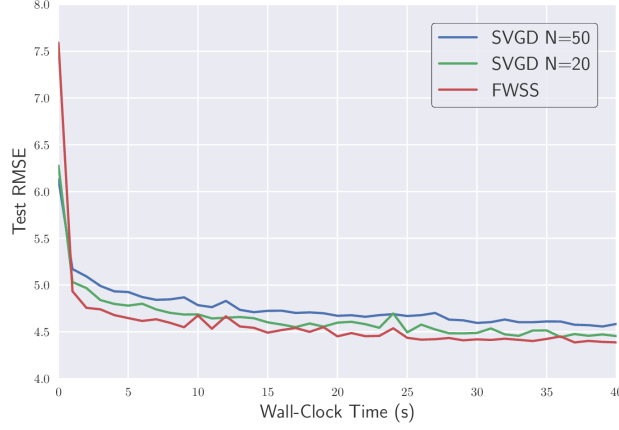
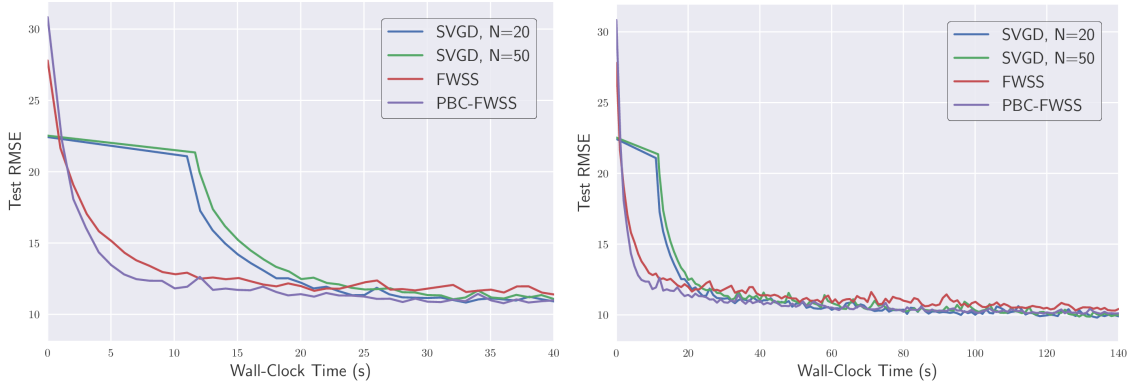


Figure 7: [Comparison of FWSS and SVGD in terms of wall clock time with test accuracy(Protein data)]



(a) Comparison in terms of wall clock time with test RMSE

(b) Comparison in terms of wall clock time with test RMSE

Figure 9: Comparison in the logistic regression model

H Stein Points Experiments

The stein pints method utilizes two algorithms for the objective function, the greedy algorithm and the herding algorithm. In order to perform optimization, the authors indicate three methods: the Nelder-Mead method, the Monte Carlo method and the grid search method. To perform on step optimization in an n dimension parameter space, the Nelder-Mead method needs to evaluate the objective function at least $n + 1$ times, and the grid search method needs to evaluate d^n times, where d is the number of the grids in one dimension.

We conducted toy experiments to approximate Gaussian mixtures in 6 different combinations. The result shown in Fig. 10 is not favorable as expected. First, the data points needs to be bounded in a specifically designed area, which is

not trivial and may require more time than usual. Second, it failed to capture the characteristic of the target distribution since it only does exploration. Since the greedy algorithm together with Monte Carlo seems to perform the best fit, we use this setting in the bayesian logistic regression experiment.

The details of the greedy algorithm is elaborated as follows. The distance we want to minimize between n sampled points and the target distribution is defined as

$$D = \sqrt{\frac{1}{n^2} \sum_{i,j=1}^n k_0(x_i, x_j)}.$$

Starting from the first MAP data point, the greedy algorithm tries to find a data points that minimize the distance. The greedy algorithm solves the optimization problem

$$x_n = \operatorname{argmin}_x \frac{k_0(x, x)}{2} + \sum_{i=1}^{n-1} k_0(x_i, x)$$

for the n th data point, where $k_0(x, x')$ is the Stein reproducing kernel defined as

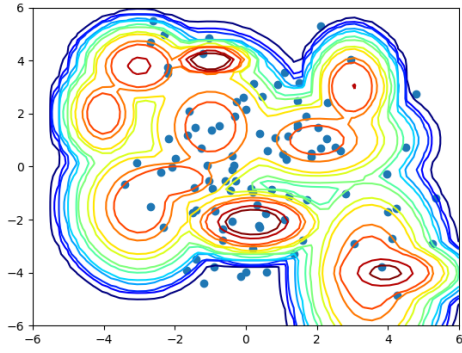
$$k_0(x, x') = \nabla_x \cdot \nabla_{x'} k(x, x') + \nabla_x k(x, x') \cdot \nabla_{x'} \log p(x') + \nabla_{x'} k(x, x') \cdot \nabla_x \log p(x) + k(x, x') \nabla_x \log p(x) \nabla_{x'} \log p(x'). \quad (30)$$

The Gaussian kernel is used for the base kernel $k(x, x')$.

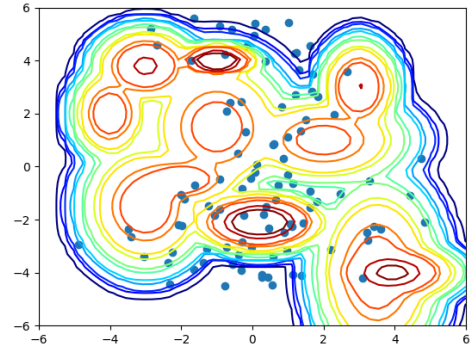
The details of the Monte Carlo methods is elaborated as follows. The first sample is drawn by performing MAP approximation, for which we looped 100 times. From the second sample, we take the strategy below. First, we uniformly select 20 base points within existing points. Then, we sample 20 points from a Gaussian distribution, whose location is the base point and scale is set to be 1. We resampled the points until the elements of the 20 points all fall in the range $[-1, 1]$. Finally, we evaluate the 20 points and select the one performs the best.

However, the experiment is hardly feasible. Sampling only 4 data points took 3 minutes and the accuracy is only 56%.

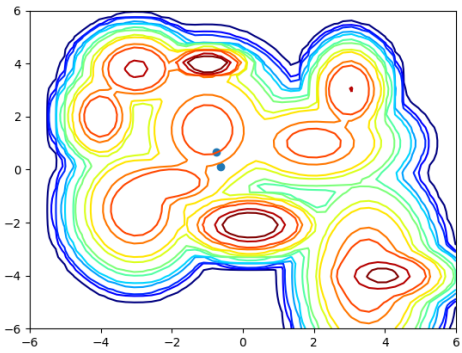
We also tried to test the method on bayesian neural network settings. However, it is not realistic since the dimension of the parameter space is too large.



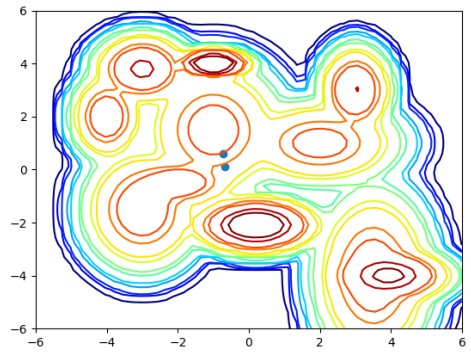
(a) Greedy Monte Carlo



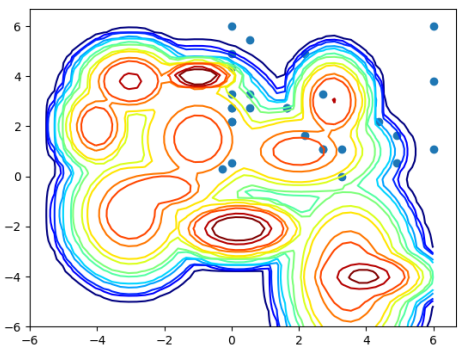
(b) Herding Monte Carlo



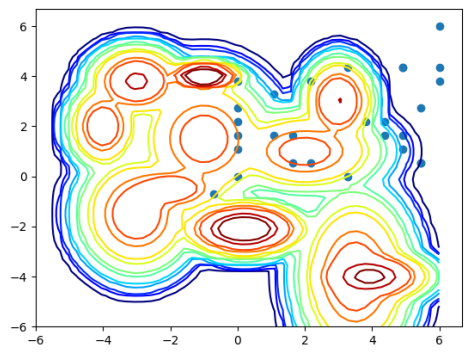
(c) Greedy Nelder-Mead



(d) Herding Nelder-Mead



(e) Greedy Grid Search



(f) Herding Grid Search

Figure 10: Plots of the toy experiment

I Cache-FWSS

As we had discussed in the main paper of Section 4.1, we can combine FWSS and SVGD. The algorithm is simple. We just replace the Approx-LMO in FWSS by Cached approx-LMO as described in Alg. 7. To use the Cached approx-LMO, we first optimize N particles by SVGD. After finishing the SVGD, we store the optimized particles in the “Cache”. Then, in the Cached approx-LMO, in each iteration, we first choose the particle which minimize the absolute value of $\nabla_x \text{MMD}(x)^2$ from the Cache. Then we adapt the chosen particle as the initial state of the solution, and update it. By doing this, the number of iteration will be drastically small for each iteration. And we eliminate the chosen particle from the cache to prevent from choosing the same particle for many times. Based on this Cached approx-LMO, the whole algorithm is given in Alg. 8. We name this algorithm, Cache-FWSS. When we use all the particles which are obtained by SVGD, then we will use the usual Approx-LMO in the Algorithm. The theoretical property of this algorithm is apparently as same as the FWSS.

Algorithm 7: Cached approx-LMO

```

1: Input:  $\mu_p^{(k)}$ 
2: Output:  $k(\cdot, x^{L+1})$ 
3:  $x^{(0)} = \operatorname{argmin}_{x \in \text{cache}} |\nabla_x \text{MMD}(x)|^2$ 
4: Eliminate the chosen  $x$  from the Cache
5: for  $l = 0 \dots L$  do
6:   Compute  $\nabla_x \text{MMD}^2$  by Eq.(4)
7:   Update  $x^{(l+1)} \leftarrow x^{(l)} + \epsilon^{(l)} \cdot \nabla_x \text{MMD}^2$ 
8: end for

```

Algorithm 8: Cached Frank Wolfe Stein Sampling

... as Arg 3, except for the input of step 1 and use the Cached approx-LMO at step 3.
Input: A target density $p(x)$ and particles $\{x_n^{(0)}\}_{n=1}^n$ obtained by SVGD
 $\bar{g}_n = \text{Cached approx-LMO}(\mu_p^{(n)})$

We did the numerical experiment about this algorithm on the toy data which we had explained in the previous section. First we optimized 200 particles by SVGD. We set the number of iteration $L = 10$ in Cached approx-LMO. The results are shown in Fig 11.

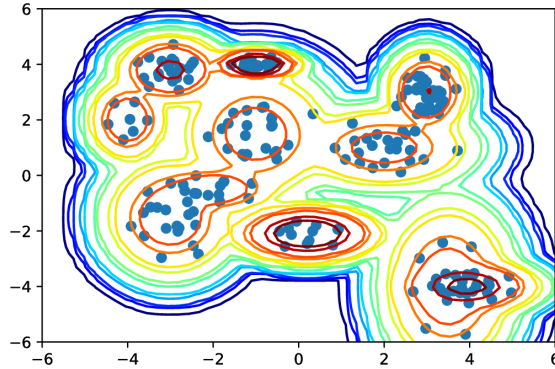


Figure 11: Toy data results by Cached-FWSS

J Lazy Frank-Wolfe algorithm

As we had mentioned in the main paper, we can utilize the many variants of the FW to our setting. Here we pick up the Lazy FW [6].

In Lazy FW, instead of calling the LMO at each step, we re-use the particles which had already been processed and stored if some of them satisfy the specified criterion. We call such a procedure as Lazy-LMO and shown in Alg 9. Actually, this method never improves the sample complexity of the bound, however it drastically reduce the wall-clock time. When no stored particles satisfy the criterion, we will solve the LMO or update the criterion. When we solve the LMO, we use the Chached approx-LMO of Alg. 7 which also contribute to the drastic reduction of the wall clock time of approximate LMO calculation.

To skip the calling of the LMO, we have to calculate the criterion. To calculate the criterion, we need to calculate the following expression, which is often called the duality gap,

$$\begin{aligned} \text{Dg}(\mu_{\hat{p}}^{(n)}, x) &:= \langle \mu_{\hat{p}}^{(n)} - \mu_p, \mu_{\hat{p}}^{(n)} - \Phi(x) \rangle \\ &= \sum_{l', l=0}^{n-1} w_{l'}^{(n-1)} w_l^{(n-1)} k(x_{l'}, x_l) - \sum_{l=0}^{n-1} w_l^{(n-1)} (k(x_l, x) + \mu_p(x_l)) + \mu_p(x). \end{aligned} \quad (31)$$

The whole algorithm is given in Alg. 10, where we consider the situation that we have already pre-processed particles via SVGD to further reduce the wall clock time. We can also consider the case that particles are not processed

by SVGD. In that case, we simply initialize particles sampling from prior or randomly.

Algorithm 9: Lazy LMO

```

1: Input:  $\Phi_n, K, \mu_{\hat{p}}^{(n)}$ 
2: Output: false or  $k(\cdot, y)$ 
3: if  $x$  cached with  $\text{Dg}(\mu_{\hat{p}}^{(n)}, x) \leq -\Phi/K$  exists then
4:   return  $k(x, \cdot)$  {Cache call}
5: else
6:    $k(\cdot, x) = \text{Cached approx-LMO}(\mu_{\hat{p}}^{(n)})$ 
7:   if  $\text{Dg}(\mu_{\hat{p}}^{(n)}, x) \leq -\Phi/K$  then
8:     return  $k(x, \cdot)$  and add  $x$  to cache
9:   else
10:    return false
11:   end if
12: end if

```

Algorithm 10: Lazy Frank Wolfe Stein Sampling (Lazy FWSS)

```

1: Input: Accuracy parameter  $K$ ,
   a target density  $p(x)$ , initial particles  $\{x_n^{(0)}\}_{n=N}$  obtained by SVGD
2: Add all the initial particles into the cache.
3:  $x_0 = \text{argmin}_{x \in \text{cache}} |\nabla_x \ln p(x)|$ 
4:  $\mu_{\hat{p}}^{(0)} = k(\cdot, x_0)$ 
5:  $\Phi_0 = -\text{argmin}_{x \in \text{cache}} \text{Dg}(\mu_{\hat{p}}^{(0)}, x)/2$ 
6: for iteration  $n$  do
7:    $\bar{g}_n = \text{Lazy-LMO}(\Phi_n, K, \mu_{\hat{p}}^{(n)})$ 
8:   if  $\bar{g}_n = \text{false}$  then
9:      $\mu_{\hat{p}}^{(n+1)} = \mu_{\hat{p}}^{(n)}$ 
10:     $\Phi_{n+1} = \frac{\Phi_n}{2}$ 
11:   else
12:     $\lambda_k = \text{argmin}_{\lambda \in [0,1]} J((1-\lambda)\mu_{\hat{p}}^{(n)} + \lambda\bar{g}_n)$ 
13:    Update  $\mu_{\hat{p}}^{(n+1)} = (1-\lambda_l)\mu_{\hat{p}}^{(n)} + \lambda_n\bar{g}_n$ 
14:     $\Phi_{n+1} = \Phi_n$ 
15:   end if
16: end for

```

The theoretical behavior of this algorithm is as follows:

Theorem 5 (Consistency) *The approximate posterior mean $\hat{Z}_{f,p}$ by Alg 10 converges to the true integral $Z_{f,p}$ at the following rates*

$$|Z_{f,p} - \hat{Z}_{f,p}| \leq \text{MMD}(\{(x_n)\}_{n=1}^N) \leq \sqrt{2}de^{-\frac{N}{2}(\frac{R\epsilon}{KdL})^2} \quad (32)$$

where d is the diameter of the marginal polytope \mathcal{M} , δ is the accuracy parameter, R is the radius of the smallest ball of center μ_p included \mathcal{M} , and $\epsilon = \min_k \Phi_k$ which is positively bounded.

Theorem 6 (Contraction) *Let $S \subseteq \mathbb{R}$ be an open neighborhood of the true integral $Z_{f,p}$ and let $\gamma = \inf_{r \in S^c} |r -$*

$Z_{f,p}| > 0$. Then the posterior probability of mass on $S^c = \mathbb{R} \setminus S$ by Alg 10 vanishes at a rate:

$$\text{prob}(S^c) \leq \frac{2d}{\sqrt{\pi}\gamma} e^{-\frac{N}{2} \left(\frac{R\epsilon}{KdL} \right)^2 - \frac{\gamma^2}{4d^2} e^{\left(\frac{R\epsilon}{KdL} \right)^2 N}} \quad (33)$$

where d is the diameter of the marginal polytope \mathcal{M} , δ is the accuracy parameter, R is the radius of the smallest ball of center μ_p included \mathcal{M} , and $\epsilon = \min_k \Phi_k$ which is positively bounded.

Those proofs are shown later in this section.

Practically, we have to calculate Eq. (31) and this is difficult since this includes the integral μ_p . We tried to approximate this term by the technique of biased importance sampling [2], but not work well. Thus, practical implementation of this algorithm is the future work.

J.1 Proofs

The proof goes in the same way as FWSS and we have to be careful about how the approximate LMO describes. We use the proof of Proposition 3.2 in [3] as we did in the proof of FWSS. The notation below is the same as [3].

In the Lazy-LMO, we do not solve the LMO for every iteration but first we check whether the stored particles satisfies following condition or not,

$$\langle v_k, \tilde{w}_k \rangle \leq -\Phi_k/K. \quad (34)$$

If there exists the particle which satisfies above condition, then we do not solve the LMO but just return the particle which satisfies above condition. If no particle satisfies above condition, then we solve approximate LMO or update the accuracy parameter Φ_k following the algorithm. First we consider the case that we did not update the accuracy parameter, that is, all the procedures are consisted by only positive calls[6].

Here we assume that objective function is L/M lipshitz, where we introduced M to skip the rescaling the lipshitz constant later. Then $\|v_k\| \leq L$ holds. Thus, $\frac{1}{L} \leq \frac{1}{\|v_k\|}$ holds. When we consider the bound of $\|v_k\|^2$, then the discussion up to Eq.(12) in [3] holds by replacing all the w by \tilde{w} . And thus

$$\|v_k\|^2 = \frac{\|v_{k-1}\|^2 \|\tilde{w}_{k-1}\|^2 - \langle v_{k-1}, \tilde{w}_{k-1} \rangle^2}{\|v_{k-1} - \tilde{w}_{k-1}\|^2} \quad (35)$$

holds. When we use $-\frac{1}{L^2} \geq -\frac{1}{\|v_k\|^2}$, following relation holds

$$\begin{aligned} \|v_k\|^2 &= \frac{\|v_{k-1}\|^2 \|\tilde{w}_{k-1}\|^2 - \langle v_{k-1}, \tilde{w}_{k-1} \rangle^2}{\|v_{k-1} - \tilde{w}_{k-1}\|^2} \\ &\leq \frac{\|v_{k-1}\|^2 (\|\tilde{w}_{k-1}\|^2 - \frac{\Phi_k^2}{(LK)^2})}{\|v_{k-1} - \tilde{w}_{k-1}\|^2} \\ &\leq \left(1 - \left(\frac{\Phi_k}{KL(\|g\| + \rho_s \|M\|)} \right)^2 \right) \|v_{k-1}\|^2 = \left(1 - \left(\frac{\Phi_k}{C} \right)^2 \right) \|v_{k-1}\|^2 \end{aligned} \quad (36)$$

Here we assume that all the calls are only positive, that no negative call exists. Then following relation holds,

$$\|v_k\|^2 \leq \|v_0\|^2 e^{-\frac{1}{C^2} \sum_{l=0}^k \Phi_k} \leq \|v_0\|^2 e^{-\frac{k}{C^2} \min_k \Phi_k} \quad (37)$$

However as shown by Theorem 4.1 in [6], it is impossible to construct the algorithm that no negative call exists and the number of successive positive call are bounded. Fortunately, now we want to bound the objective function by the number of particles not the iteration of the algorithm, this is different from [6]. And the number of particles increases only when the positive call are used. This means we can use the bound of Eq.(37) directly. And as shown in theorem 4.1 in [6], the number of negative call is also bounded, that is the lazy algorithm surely increase the number of particles and the situation that no positive call exists does not occur.

By definition, the value of $\min_k \Phi_k$ is positively bounded and thus the theorem directly obtained in the same way as the proof of FWSS. Above proof is about the line search, but we can show the variant of constant step and fully correction easily by the same discussion with FWSS.

The value of Lipschitz constant is, our objective function is $J(\mu_{\hat{p}}) = \frac{1}{2} \|\mu_p - \mu_{\hat{p}}\|_{\mathcal{H}}^2$, and thus

$$L_k = \max_{g \in \mathcal{M}} \langle \mu_{\hat{p}}^{(k)} - \mu_p, g \rangle = \max_x \sum_{l=0}^k w_l^{(k)} k(x_l, x) - \int k(x', x) p(x) dx \quad (38)$$

and the lipschitz constant becomes $L = \max_k L_k$

About the contraction theorem, we can prove it in the same way as FWSS.

K Quadrature rules

K.1 Herding and Quadrature

When exact integration cannot be done, we often resort to use the quadrature rule approximations. A quadrature rules approximate the integral by weighted sum of functions at the certain points,

$$\hat{Z}_{f,p} = \sum_{n=1}^N w_n f(x_n), \quad (39)$$

where we approximated $p(x)$ by $\hat{p}(x) = \sum_{n=1}^N w_n \delta(x_n)$ and $\delta(x_n)$ is a Dirac measure at x_n . There are many ways to specifying the combination of $\{(w_n, x_n)\}_{n=1}^N$. In this paper, we call w_n s as *weights* and x_n s as *particles*. Most widely used quadrature rule is the Monte Carlo(MC). We simply set all the $w_n = \frac{1}{N}$ and we produce x_n s by drawn from $p(x)$ randomly. This non-deterministic sampling based approximation converges at a rate $\mathcal{O}(\frac{1}{\sqrt{N}})$. On the other hand, in the Quasi Monte Carlo, we decide x_n s to directly minimize the some criterion.

In the kernel herding method [9, 1], the discrepancy measure is the Maximum Mean Discrepancy (MMD). Let \mathcal{H} be a Hilbert space of functions equipped with the inner product $\langle \cdot, \cdot \rangle_{\mathcal{H}}$ and associated norm $\| \cdot \|_{\mathcal{H}}$. The MMD is defined by

$$\text{MMD}(\{(w_n, x_n)\}_{n=1}^N) = \sup_{f \in \mathcal{H}: \|f\|_{\mathcal{H}}=1} |Z_{f,p} - \hat{Z}_{f,p}| \quad (40)$$

If we consider \mathcal{H} be a reproducing kernel Hilbert space(RKHS) with a kernel k . In this setup, we can rewrite the MMD using $k(x, x')$ and set all the $w_i = \frac{1}{N}$,

$$\begin{aligned} & \text{MMD}^2(\{(w_i = \frac{1}{N}, x_i)\}_{i=1}^N) \\ &= \sup_{f \in \mathcal{H}: \|f\|_{\mathcal{H}}=1} |Z_{f,p} - \hat{Z}_{f,p}|^2 = \|\mu_p - \mu_{\hat{p}}\|_{\mathcal{H}}^2 \\ &= \iint k(x, x') p(x) p(x') dx dx' - 2 \iint k(x, x') p(x) \hat{p}(x') dx dx' + \iint k(x, x') \hat{p}(x) \hat{p}(x') dx dx' \\ &= \iint k(x, x') p(x) p(x') dx dx' - 2 \frac{1}{N} \sum_{n=1}^N \int k(x, x_n) p(x) dx + \frac{1}{N^2} \sum_{n,m=1}^N k(x_n, x_m) \end{aligned} \quad (41)$$

where $\mu_p = \int k(\cdot, x) p(x) dx \in \mathcal{H}$. The herding algorithm greedily minimize the above discrepancy in the following way,

$$\begin{aligned} x_{N+1} &\leftarrow \arg \min_x \left[\text{MMD}^2(\{(w_n = \frac{1}{N+1}, x_n)\}_{n=1}^N, (w_{N+1} = \frac{1}{N+1}, x)) \right] \\ &= \arg \max_x \left[\frac{2}{N+1} \int k(x, x') p(x') dx' - \frac{2}{N+1} \sum_{n=1}^N k(x, x_n) \right] \end{aligned} \quad (42)$$

It is widely known that, under certain assumption, they converges at a rate $\mathcal{O}(\frac{1}{N})$.

K.2 Bayesian Quadrature

In the Bayesian Quadrature method [12, 16], we put on the Gaussian process prior on f with kernel k and mean 0. In usual gaussian process, after conditioned on $f(X) = (f(x_1), \dots, f(x_N))^T$, we can obtain the closed-form posterior distribution of f ,

$$p(f(x_*)|p(f(X))) = N(f(x_*)|\mu, \Sigma), \quad (43)$$

where $\mu = k(x_*, X)K^{-1}f(X)$, $\Sigma = k(x_*, x_*) - k(x_*, X)K^{-1}k(X, x_*)$, here $K_{i,j} = K(x_i, x_j)$ and $N(x|\mu, \Sigma)$ means the Gaussian distribution with mean μ and the covariance Σ . Thanks to the property of Gaussian process that linear projection preserves the normality, the integrand is also Gaussian, and thus we can obtain the posterior distribution of the integrand as follows,

$$\begin{aligned} \mathbb{E}_{\text{GP}}[Z_{f,p}] &= \mathbb{E}_{\text{GP}} \left[\int f(x)p(x)dx \right] \\ &= \iint f(x)p(f(x)|p(f(X)))p(x)dxdf = \int k(x, X)K^{-1}f(X)p(x)dx \\ &= \mathbf{z}^T K^{-1}f(X) \end{aligned} \quad (44)$$

where $\mathbf{z}_n = \int k(x, x_n)p(x)dx$. From the above expression,

$$\mathbb{E}_{\text{GP}}[Z_{f,p}] = \sum_{n=1}^N w_{\text{BQ}}^{(n)} f(x_n), \quad w_{\text{BQ}}^{(n)} = \sum_m z_j^T K_{nm}^{-1}. \quad (45)$$

This is different from the herding where we set $w_n = \frac{1}{N}$. In the same way as the expectation, we can calculate the variance of the posterior,

$$\mathbb{V}[Z_{f,p}|f(x_1), \dots, f(x_N)] = \iint k(x, x')dx dx' - \mathbf{z}^T K^{-1} \mathbf{z} \quad (46)$$

[16] proved that in the RKHS setting, minimizing the posterior variance corresponds to minimizing the MMD,

$$\mathbb{V}[Z_{f,p}|f(x_1), \dots, f(x_N)] = \text{MMD}^2(\{(w_{\text{BQ}}^{(n)}, x_n)\}_{n=1}^N). \quad (47)$$

The BQ minimize the above discrepancy greedily in the following way,

$$x_{N+1} \leftarrow \arg \min_x \mathbb{V}[Z_{f,p}|f(x_1), \dots, f(x_N), f(x)]. \quad (48)$$

[16] showed that

$$\text{MMD}(\{(w_{\text{BQ}}^{(n)}, x_n)\}_{n=1}^N) = \inf_{w \in \mathbb{R}^N} \sup_{f \in \mathcal{H}: \|f\|_{\mathcal{H}}=1} |Z_{f,p} - \hat{Z}_{f,p}| \quad (49)$$

and thus,

$$\text{MMD}(\{(w_{\text{BQ}}^{(n)}, x_n)\}_{n=1}^N) \leq \text{MMD}(\{(w_n = \frac{1}{N}, x_n)\}_{n=1}^N) \quad (50)$$

The finite sample bound of BQ was studied in [7] by using the Frank-Wolfe algorithm which will be explained in the next chapter.